Computers & Geosciences 88 (2016) 83–96

Contents lists available at ScienceDirect

Computers & Geosciences

journal homepage: www.elsevier.com/locate/cageo

Case study

Computation of the gravity field and its gradient: Some applications

C.P. Dubey [a], V.M. Tiwari [a,b,*]

[a] CSIR-National Geophysical Research Institute, Hyderabad, India
[b] ESSO-National Centre for Earth Science Studies, Thiruvananthapuram, India

ARTICLE INFO

Article history:
Received 11 June 2015
Received in revised form
7 October 2015
Accepted 10 December 2015
Available online 17 December 2015

Keywords:
Gravity
Gravity gradient
MATLAB
Rectangular body
Airborne gravity gradiometry

ABSTRACT

New measuring instruments of Earth's gravity gradient tensors (GGT) have offered a fresh impetus to gravimetry and its application in subsurface exploration. Several efforts have been made to provide a thorough understanding of the complex properties of the gravity gradient tensor and its mathematical formulations to compute GGT. However, there is not much open source software available. Understanding of the tensor properties leads to important guidelines in the development of real three dimensional geological models. We present a MATLAB computational algorithm to calculate the gravity field and full gravity gradient tensor for an undulated surface followed by regular geometries like an infinite horizontal slab, a vertical sheet, a solid sphere, a vertical cylinder, a normal fault model and a rectangular lamina or conglomerations of such bodies and the results are compared with responses using professional software based on different computational schemes. Real subsurface geometries of complex geological structures of interest are approximated through arrangements of vertical rectangular laminas. The geological application of this algorithm is demonstrated over a horst-type structure of Oklahoma Aulacogen, USA and Vredefort Dome, South Africa, where measured GGT data are available.

1. Introduction

The Earth's gravity and gravity gradient anomalies provide important information for delineating geological structures of economic importance. The gravity gradient method is one of the geophysical tools used successfully to detect remote occurrences of target bodies and to define geological models with enhanced resolution. It is frequently employed in interpretation for isolating gravity anomalies (Murphy and Dickinson, 2009). The use of the gravity gradient in exploration is becoming more common in recent years due to the development of airborne gradiometry with an accuracy of ~2–5 eötvos unit (1E=0.1 mGal/km) over wavelengths of ~45 m (Dransfield and Christensen, 2013; Zuidweg and Mumaw, 2007) or ~100 km for the ongoing gradiometer satellite mission called GOCE (Herceg et al., 2014; Godah and Krynski, 2011), which can give a potential map easily over large, highly inaccessible undulating regions. Gravity gradiometers measure gradients of the gravity vector components in three Cartesian directions (Fig. 1) and measured components are used to produce the nine – component tensor, T_{ij}. Since the gravitational potential satisfies Laplace's equation, the trace of the symmetric tensor is equal to zero. Thus, there are only five independent elements (e.g., T_{xx}, T_{xy}, T_{xz}, T_{yy}, and T_{yz}) as $T_{ij}=T_{ji}$, where $i\neq j$. Furthermore, the T_{zz} component is often displayed as it closely relates to the subsurface geology (Pedersen and Rasmussen, 1990).

Conventional gravity data show the strength of the earth's gravity field but are less sensitive to the edges of bodies and contain no directional information. In contrast, gravity gradients directly recover sharp signal over the edges of structures and are closely related to the edges, corners, and center of mass of the causative bodies producing complex pattern of anomalies. For a simple positive density cube, a classic gravity map would show a diffused circular anomaly centered over the body. In contrast, the six gravity gradients provide a powerful tool for delineating the shape of the body (Saad, 2006). The vertical tensor component T_{zz} provides an estimate of maximum depth and predicts boundary information directly related to the geological body and the other components give close information related to the geometry of the body. The T_{xx} component effectively indicates the eastern and western edges of a feature, whereas the T_{yy} component indicates the northern and southern edges. The T_{xz} component divides the body into eastern and western halves approximately symmetrically and gives the central anomaly axis towards north–south direction; similarly T_{yz} component divides the body into northern and southern halves symmetrically and gives the central anomaly axis towards east–west direction. It also helps to show north–south and east–west trending edges. The T_{xy} component gives information about the four corners of near rectangular bodies and locates the center point of symmetrical bodies in case of alignment

* Corresponding author at: CSIR-National Geophysical Research Institute, Hyderabad, India.
E-mail addresses: virendra.m.tiwari@gmail.com, vmtiwari.ncess@gov.in (V.M. Tiwari).

http://dx.doi.org/10.1016/j.cageo.2015.12.007
0098-3004/

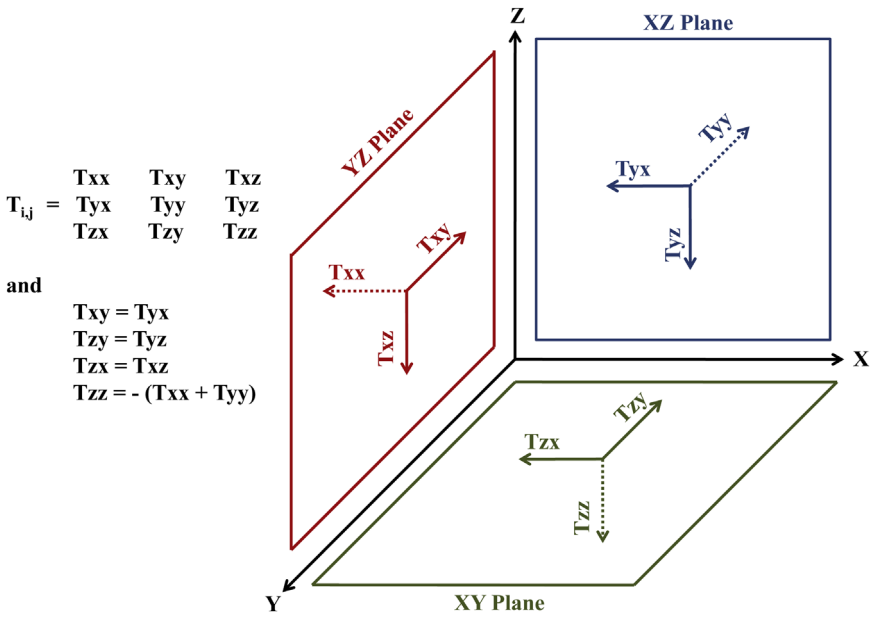

Fig. 1. Schematic diagram showing the gravity field vector G_x, G_y, G_z and full gravity gradient tensor components T_{xx}, T_{xy}, T_{xz}, T_{yy}, T_{yz} and T_{zz}.

of geological body with *x* and *y* directions.

2. Commutating gravity and its gradients for geological structures

In particular, gravity and gravity gradient data explore the subsurface geology originating from mass distribution in subsurface. Therefore, estimating the model parameters of causative sources such as location, depth, thickness, size, shape, extension, density variations etc., has a key importance in the interpretation stage. However the well-known complex nature of the full gravity gradient tensor (FTG) may quite complicate the interpretation procedure compare to the gravity alone (Saad, 2006). Therefore, for better understanding of the complex nature of FTG, it is thought to provide a detail discussion on computational algorithms of three dimensional regular shaped geometries and their behavior for the gravity field and their gradient components due to various geometrical shapes. Several researchers have proposed modeling approaches for computation of gravity and gravity gradient responses due to homogeneous polyhedral bodies (Okabe, 1979; Gotze and Lahmeyer, 1988; Barnet, 1976; Coggon, 1976; Pohánka, 1988; Yao and Changli, 2007). Bhattacharya (1964), Nagy (1966), and Plouff (1976) presented closed form mathematical equations for prism shaped bodies, whereas Talwani and Ewing (1960) and Talwani (1965) used numerical integration techniques for the computation of the fields due to models of arbitrary shape by dividing them into polygonal prisms or laminae. Some recent studies (e.g. Tsoulis, 2012) provided a mathematical formulation for computation of the full gravity gradient tensor from a polyhedral source. The present study utilizes theory of gravity and gravity gradient effects of a rectangular prism or rectangular lamina (Talwani, 2011) and presents MATLAB algorithms for the computation of the primary gravity field and their derivatives to each coordinate direction for regular shaped geometries like the rectangular prism, dipping fault, spherical body, vertical cylinder body and two dimensional geometries like the semi-infinite horizontal slab, and dike, all of uniform density.

2.1. Computations for regular geometries

Many geological features are approximated by 2D models like an infinite dike or a geological contact for computational simplifications. The interpretation of 2D and 2.5D potential field models is simple but might be far from reality since the real geological bodies are mostly three dimensional structures. Following sections discusses both two dimensional and three dimensional geometries with an emphasis on the three dimensional regular shaped geometries used in analyzing asymmetrical three dimensional arrangements in the subsurface. Each of the geometrical bodies used is of uniform density, although in many geological situations, the density of a particular structure may vary. This is particularly true in sedimentary rocks where the density increases with depth as a result of compaction. Often, this may be allowed using simple functional forms to approximate the density variation with depth as well as its lateral variations. However, for the purpose of this paper, the model assumes constant density for each element of a model and variations in density are simulated by the use of separate elements.

2.2. Geometries: semi-infinite horizontal slab and vertical sheet/dike

For many exploration purposes, it is common to assume that the body producing a gravity anomaly is two dimensional in nature. In particular, the removal of one spatial dimension allows greater complexity to be built into the remaining two dimensions of the model as well as making the computation of the simulation faster. Also mineralized zones are often found over linear features like shear zones, faults and so on that can be approximated as two directional features. The gravity gradients in the two-dimensional case are quite simple, since the tensor has only four components with the off-diagonal components equal by symmetry of the tensor and the diagonal elements equal in magnitude but opposite in sign (Dransfield, 1994). The potential at a point much closer to the center of the elongated body than its end is independent of the distance to the ends and therefore the components of gravity and gravity gradients in that direction are zero.

Here, we present the gravity and horizontal gradient response for two simple geometries: the semi-infinite horizontal sheet and the vertical sheet (Fig. 2). Their analytical expressions are

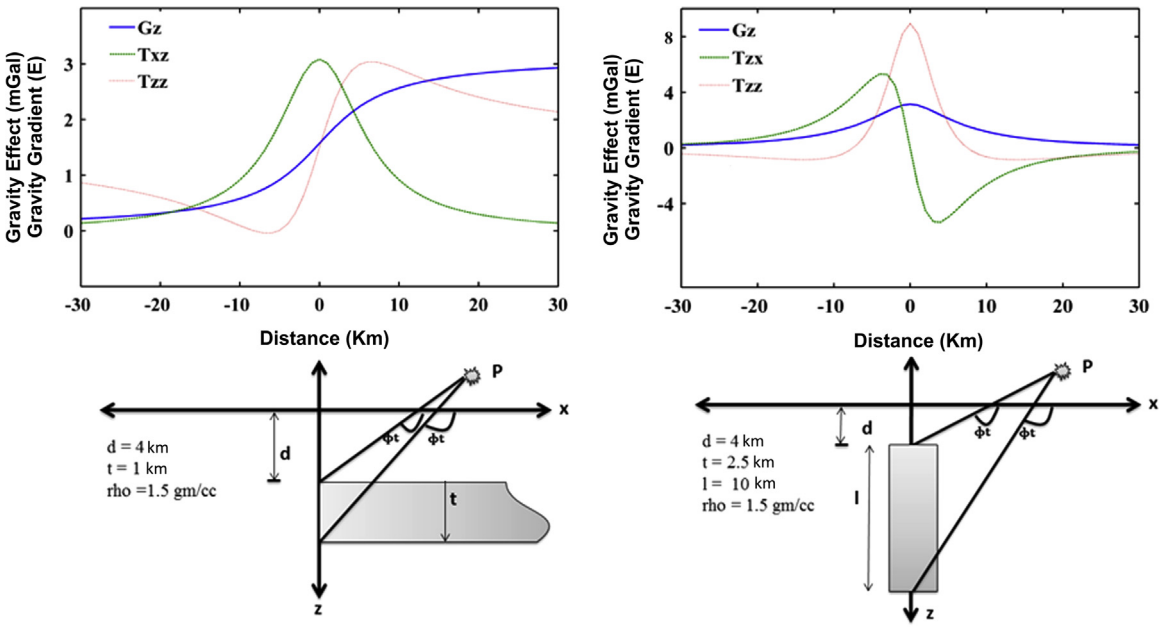

Fig. 2. Computed gravity and its horizontal gravity gradients for a 2D geometries like semi-infinite horizontal slab and vertical sheet as dike.

presented in the Appendix A. The semi-infinite horizontal sheet serves to approximate small faults of long strike. For such a sheet with thickness of 1 km at the depth of 4 km and density 1.5 g/cm^3, the computation algorithm (*mfile named as slab.m*) is developed to calculate the gravity field G_z and its gradients T_{xz} and T_{zz}. The vertical and the horizontal gradient are both infinite in this case. The maxima of the vertical component of gravity field lies at the altitude of the measurements above the edge of the sheet (Fig. 2, left). Further, the vertical sheet is useful for modeling dikes. For a vertical sheet of thickness 2.5 km with density of 1.5 g/cm^3 at the depth of 4 km extended upto 14 km, the computation algorithm (*mfile named as dike.m*) is developed to calculate the gravity field G_z and its gradients T_{xz} and T_{zz} (Fig. 2, right).

2.3. 3D geometries: rectangular lamina or prism

The gravity field of an arbitrary source is simply the point source field integrated over the volume of arbitrary source. Such computations require different type of polyhedra to approximate the arbitrary source. The expressions are directly useful for estimating the gravity field and its full gravity gradient tensor due to confined bodies in nature; particular examples range from thick massive sulfide ore bodies to salt domes (Dubey et al., 2014). The rectangular lamina or prism is a useful three dimensional body because of the ease with which more complex bodies of arbitrary source can be built from the sets of prism similar to toy building blocks; in particular, regular shaped geometric models usually consist of a volume divided by a three dimensional grid into right rectangular prism, each assigned a fixed density. The utility of the prism model has been long recognized, with the derivation of the expression for the vertical component of gravity field for a right rectangular prism published by Nagy (1966) (see also Dransfield, 1994; Talwani, 2011) and for a dipping prism by Hjelt (1974). The formulas for the complete set of gradient components for modeling in the present paper are shown in the Appendix A. Although these expressions are complex, it is a straightforward matter to use them in MATLAB program. Some care like step size must be taken with singularities at points which intersect projections of the prism sides onto the plane.

Let Q be a point with coordinate (x', y', z'), within a rectangular prism of uniform density of 2.7 g/cm^3 with its geometry at the origin of coordinate system including dimensions a in the x direction, b in the y direction and d in the z direction as shown in Fig. 3.1(a). The gravity field and full gravity gradient tensor are computed using a MATLAB computational algorithm (*mfile named as prism.m*) away from the prism, at point R, with coordinate (x, y, z) and at distance $r=[(x-x')^2+(y-y')^2+(z-z')^2]^{1/2}$ from Q as shown in Fig. 3.1(b–j). Fig. 3.1 shows the mapped gravity field and its gradient due to a cube of positive density contrast at a plane of constant 1000 m. The cube has its edge aligned with the axis in the directions of the measurements and it is below the plane of measurement. The computed map is plotted in coordinates scaled by the distance to the top of the cube in the same scaled units with the length of each side of cube as 8 km, 4 km, and 1 km along x, y and z directions respectively. These maps have obvious similarities in shape, in relative signal amplitude with those due to the sphere. Despite these similarities, the gradient maps are clearly due to a source with square cross sections; a fact considerably less obvious in normal gravity maps. The advantage of each component of full gravity gradient for a prism can be easily identified by their prism edges. This complex behavior of gravity and gradients are shown in view map of Fig. 3.2. Particularly striking is the mapping of the cube edges by its invariants in the form of different combinations of gravity gradient components (see next section) as shown in Fig. 5. This improved spatial resolution is a natural consequence of the greater sensitivity of the gradients to the smaller features which control the detailed shape of the source. There is also a disadvantage for simulation work that the regular shaped three dimensional models constructed from right rectangular prisms require smaller mesh widths in the constituent prism than would be necessary for the modeling of the field. This means a greater number of elements and a consequent increase in computation time shows as an inevitable implication of the greater sensitivity.

For the validation, the gravity and gradient responses of the prism are computed at all points in a space of a given grid with sample spacing of 150 m in both x and y directions over the finite rectangular prism with 6 rectangular face (a special case of the homogeneous polyhedral body). The responses caused by this model are contributed by all surfaces of cubical body extending from $x=4$ units to 12 units, $y=-2$ units to 2 units and $z=1$ unit to 3 units, over the region extending from $x=0$ unit to 16 units, $y=-10$ units to 10 units for $z=0$, i.e. at a distance of 1 unit from

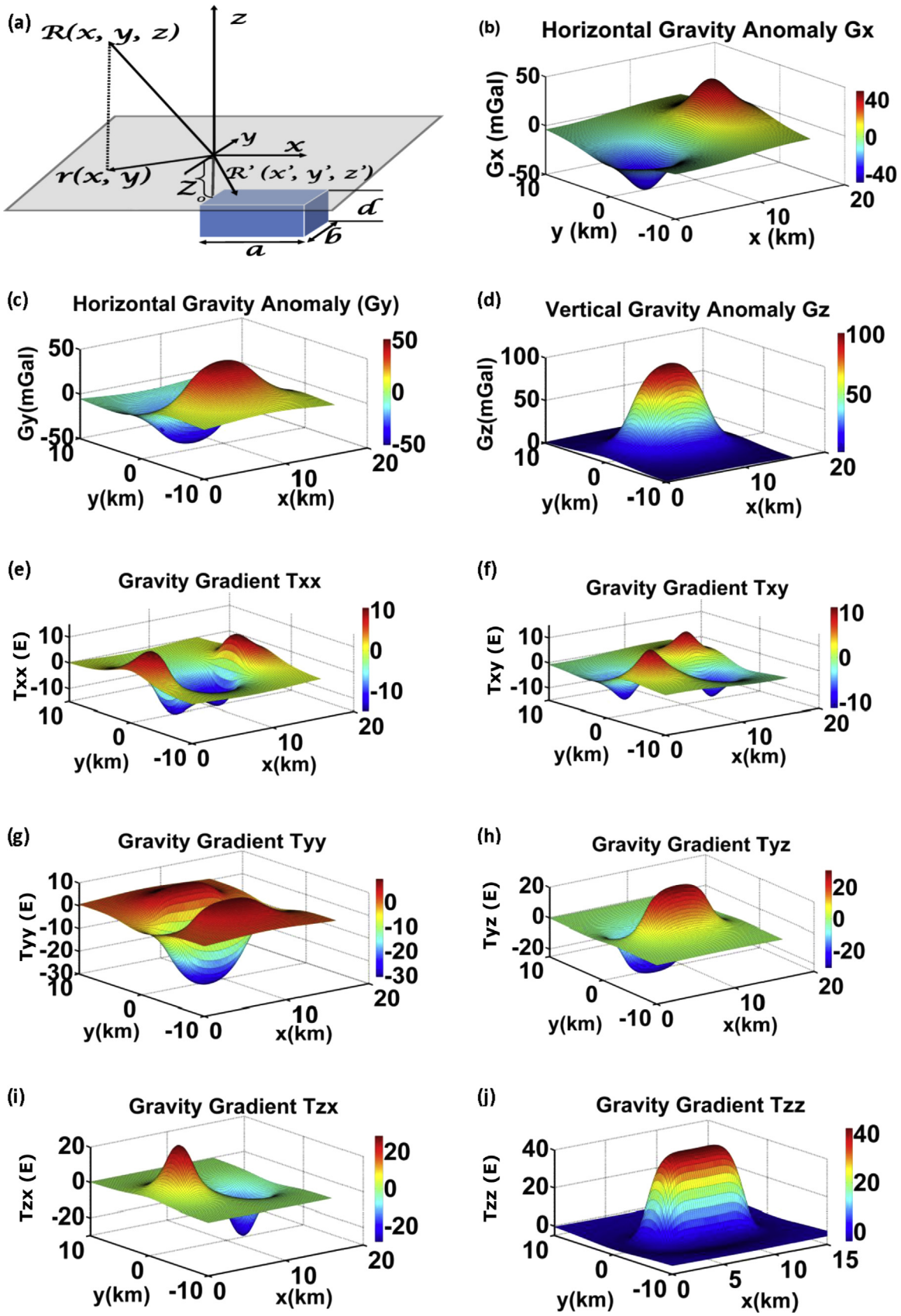

Fig. 3.1. (a)A model containing a prism and (b–d): corresponding gravity vector components and (e–j) GGT components with sampling interval of 0.2 km in *x* and *y* directions.

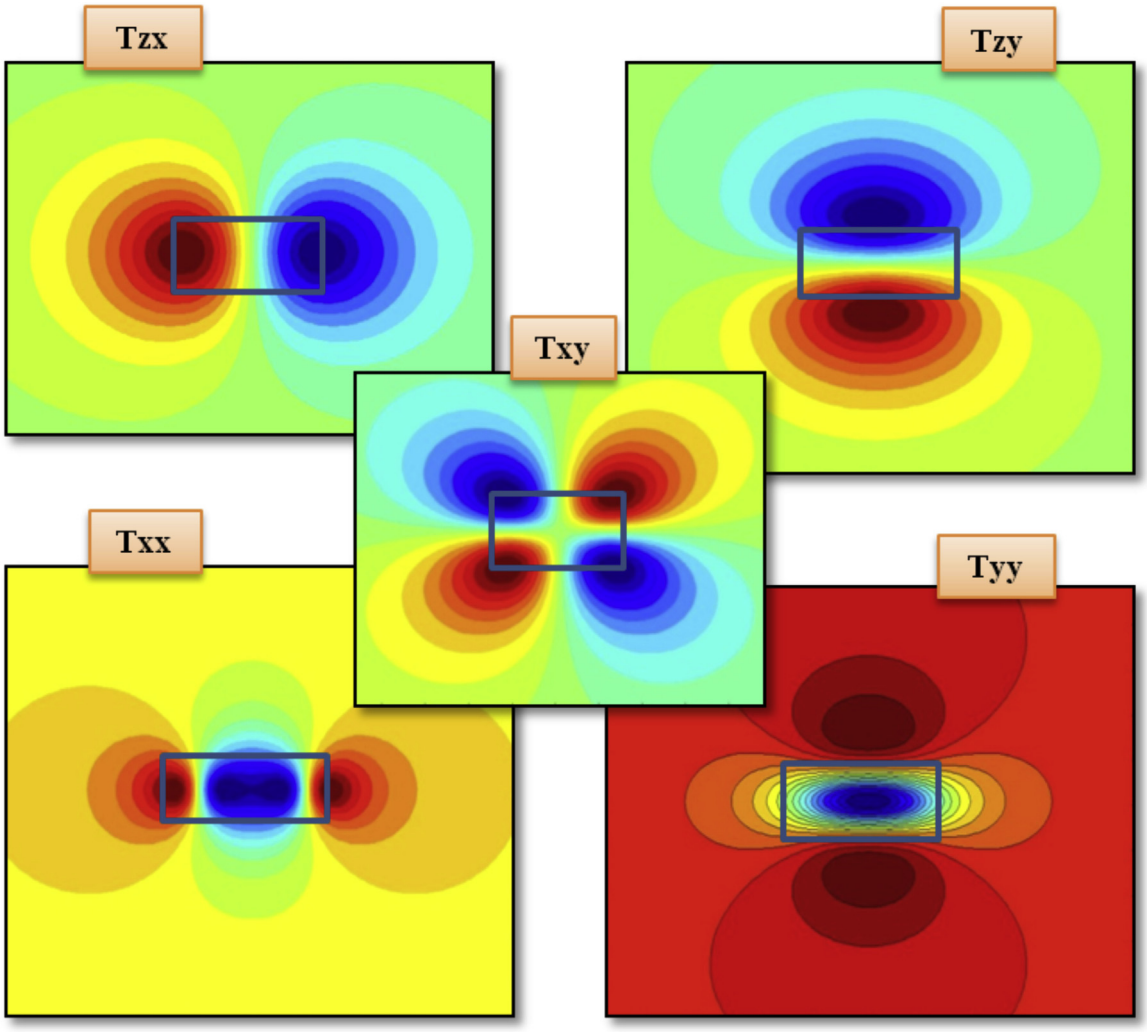

Fig. 3.2. A map view of complex behavior of gravity gradients for prism model shown in Fig. 3.1(a).

the top surface of the cuboid. For practical purposes, here 1 unit is taken equal to 1 km. The result of rectangular prism is compared with the GGT components calculated using 3D IGMAS (Schmidt and Gotze, 1998). Fig. 4 shows that the GGT components calculated using our code is as same as the IGMAS results with rms error of 0.0198 mGal, 0.0067 eötvos, 0.0151 eötvos and 0.0095 eötvos for gravity field G_z, gravity gradient T_{zx}, T_{zy} and T_{zz} respectively.

2.4. Invariants of prism

Many combinations of the gravity gradient can be used to simplify the complex pattern like mono polar, doublet, triplet, and quadruplet. The invariants of gradients are calculated, which remain unchanged under the rotation of the coordinates and help in the interpretation of the data. In the present study, three invariants of gradient are shown (Fig. 5) to illustrate the complex pattern anomalies due to the prism model.

The differential curvature magnitude (DCM) which is also known as the horizontal directive tendency is computed by a combination of other components of tensor T_{xx}, T_{xy} and T_{yy}. It emphasizes greatly the effects of shallower sources (Saad, 2006); the horizontal gradient magnitude (HGM) of G_z can be computed from the horizontal derivative components of G_z and can be used as edge detector or to map the body outline as it verifies the prism boundaries (Fig. 5), and the total gradient magnitude (TGM) is computed from the three derivatives of vertical component of gravity G_z i.e. T_{zx}, T_{zy}, and T_{zz}. The TGM is also known as the analytical signal of G_z, and can be used for depth interpretation (Saad, 2006). The mathematical expressions are mentioned below.

$$DCM = ((Txx - Tyy)^2 + 2Txy^2)^{\frac{1}{2}}$$

$$HGM = (Tzx^2 + Tzy^2)^{\frac{1}{2}}$$

$$TGM = (Tzx^2 + Tzy^2 + Tzz^2)^{\frac{1}{2}}$$

In addition to rectangular lamina or prism, we have also developed the code for a solid sphere, a vertical cylinder and a normal fault body. A MATLAB based computational algorithm (*mfile named as Sphere.m, Vcylinder.m and fault.m respectively*) is developed to analyze the gravity and full gravity gradient responses for their geometries and their mathematical expressions are given in Appendix A. The different type of geological structures can be analyzed which have distinct anomaly characteristics and that can be correlated to the structures like massive sulfide ore body, dikes, and sedimentary faults in which homogeneous beds are not substantially offset respectively.

It is very clear from the present section that 3D model calculation of regular geometries leave an impressive footprint in understanding the behavior of complex pattern of full gravity gradient tensor. From this information it is possible to build a picture of subsurface anomalies which can then be used to more

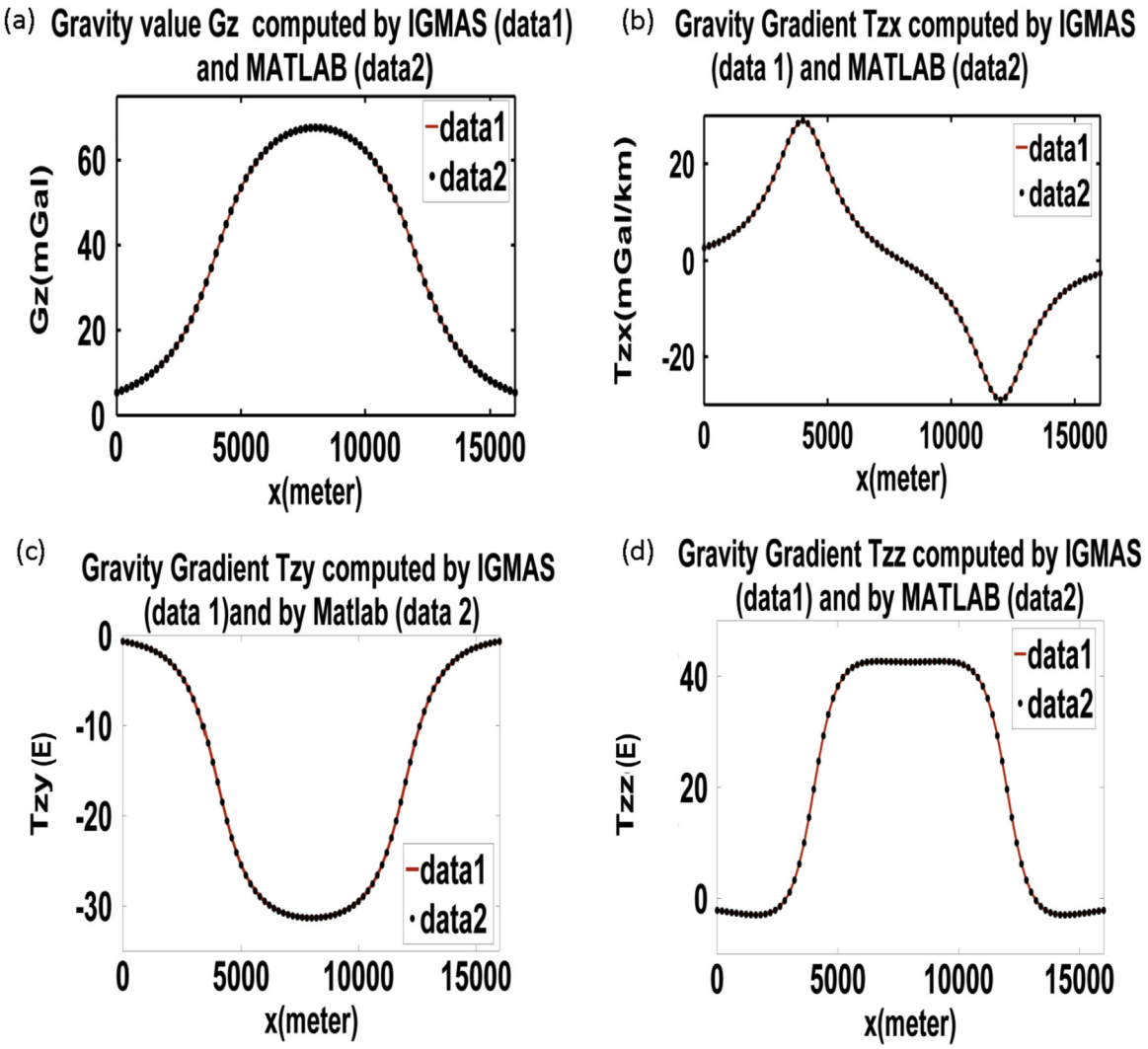

Fig. 4. (a–d) Comparison between the results acquired by our algorithm and IGMAS for the model shown in Fig. 3.1(a).

accurately target the anomalous structures associated with oil, gas and mineral deposits. However, the observed data of full gravity gradient tensor (FTG) does not seem that much easier with their complex pattern of anomalies as gravity anomaly. Therefore, following section emphasizes more in demonstrating the observed (real) FTG data with subsurface structures from different geographical areas.

3. Generation and computation of irregular shaped geometries

A MATLAB based computational algorithm (*mfile named as irregular.m*) is developed to generate any type of a body with irregular or complicated geometries using infinite cells of vertical rectangular prism, if provided topography and basement of a single layer. Then it uses the three dimensional generated geometry to compute the responses of normal gravity field and vertical gravity gradient for the same complex geometry with homogeneous density or this can be used in characterizing the response due to complex geological structures of interest. However, it may be used in the computation of lateral density variation using density function, specified by density distribution as a function of distance in volume *V* of the layer. The present program works on the assumption of fixed bottom layer and undulated upper layer as shown in Fig. 10. The demonstration of algorithm is shown in Fig. 6 that works on any gridded topographic data. In the first step of computation, program creates 6 faces of prism taking first four points A1, A2, B2, B1 as a top surface of prism fixed with same elevation of the point A1 from the given matrix data of topography and in next step it collects again four points A2, A3, B3, B2 with two common points A2 and B2 for the interface creating a second prism cell with elevation of the point A2 and it goes on as shown in Fig. 6. Therefore, it produces a total number of prisms $(i-1)\times(j-1)$ excluding end points of both vector i and j. In the last phase of the program, it computes the gravity and gravity gradient response of a set of infinitesimal prism cells associated with the undulated layer (Figs. 10 and 11). It can be easily explained from the present algorithm that the highly coarser gridded data approximates closer to the real geometry that provides the residual gravity or gravity gradient.

4. Application over two distinct geological regions

4.1. Structural analysis of Wichita uplift using rectangular prism: Horst Model

To illustrate the performance of our MATLAB code, an example was taken from the published GGT data sets collected in Southern Oklahoma Aulacogen (Keller and Baldridge, 1995). The Wichita

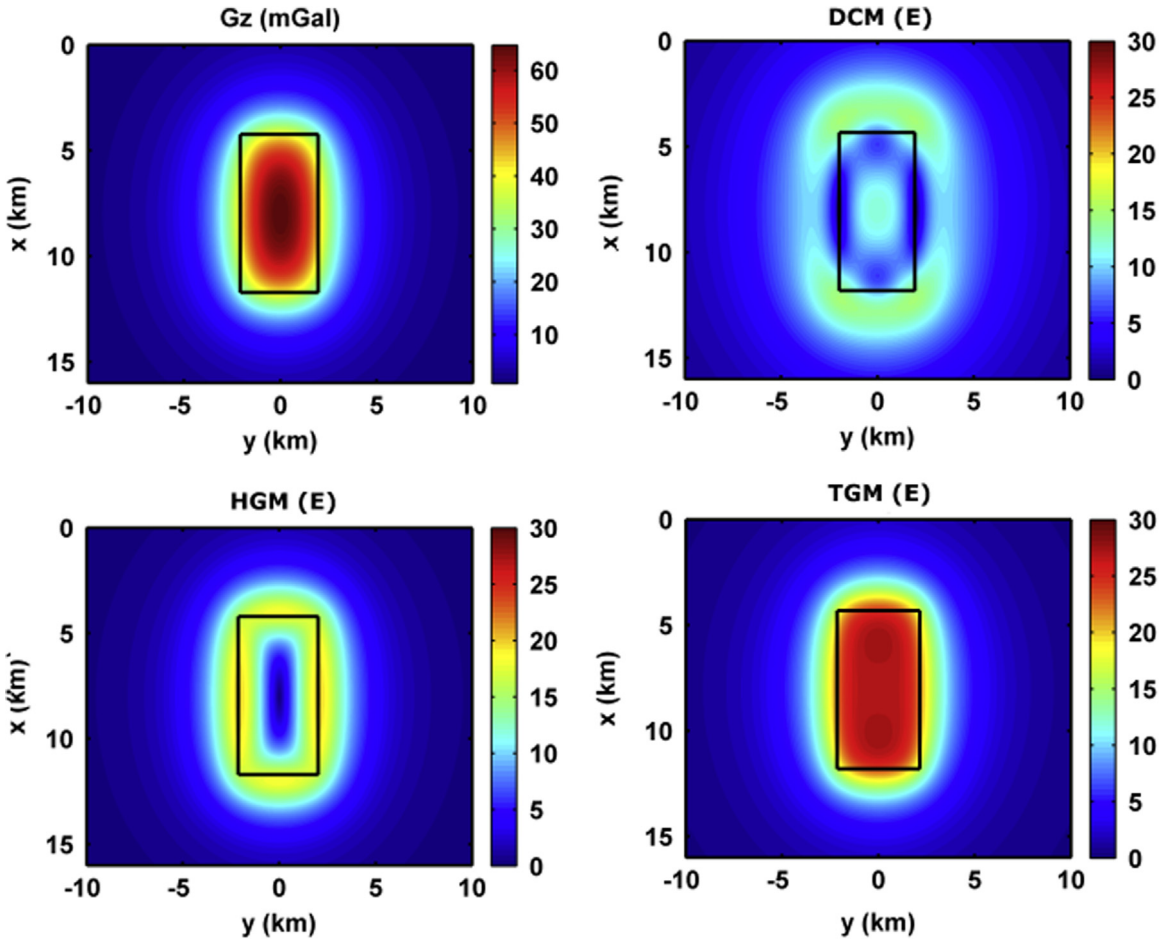

Fig. 5. Computed vertical gravity component G_z and three invariants map of HGM, DCM and TGM for given prism model in Fig. 3.1. HGM=Horizontal Gradient Magnitude, DCM=Differential Curvature Magnitude and TGM=Total Gradient Magnitude.

uplift is just south of and adjacent to the Anadarko basin (Fig. 7). The boundary between the basin and uplift is complexly faulted and abrupt. The uplift is primarily composed of Cambrian igneous rocks of diverse compositions and is part of a major structural feature that extends from northeastern Texas known as the Muenster arch, through southwestern Oklahoma to northwestern Texas, where it is known as the Amarillo uplift. Sedimentary rocks north of the Anadarko basin, in northern Oklahoma and into southern Kansas, are predominantly Paleozoic in age and probably represent facies equivalents of the sediments deposited in the basin.

Structural relations in southeastern Oklahoma are more complex. The Ardmore basin is a narrow southeast extension of the Anadarko basin. The Arbuckle–Tishamingo uplift bounds the Ardmore basin on the north, and granites in the eastern part of the uplift are the oldest exposed rocks in the area, dated as approximately 1.4 Ga (Bickford and Lewis, 1979). Cambrian igneous rocks in the western part of the uplift are similar to those in the Wichita uplift, and Paleozoic sedimentary rocks exposed in the uplift are similar to those in the Anadarko basin. The Marietta basin and Muenster arch bound the Ardmore basin on the south. Strata in the Ouachita Mountains area consist of a thick succession of folded and faulted Paleozoic sedimentary rocks, similar in age to rocks in the Anadarko and Ardmore basins. They are dominated, however, by fine-grained clastic rocks and cherts and include almost no carbonate rocks representing a deep– water environment. Late Paleozoic deformation is in the form of a major thin–skin thrusting to the north and west.

One profile AA′ (shown in Fig. 7) along north–south direction from the gravity and GGT data sets is extracted from the map of Mickus and Hinojosa (2001). This profile crosses the Wichita uplift associated with a ~35 mGal gravity anomaly shown in Fig. 8(a). Keller and Baldridge (1995) showed that this anomaly can be modeled by rectangular laminae. A trapezoidal body like a Horst model is assumed from the Keller and Baldridge (1995) and its gravity and gravity gradient responses are computed and compared with the available data. In the map, latitude and longitude are converted into kilometers by taking UTM zone 14 N (Fig. 8c).

Vertical gravity and gravity gradients responses were computed using new MATLAB – based computational algorithm with rms misfit in G_z, T_{zz}, and T_{zx} of 0.4 mGal, 6.4 eötvos, and 2.8 eötvos, respectively as shown in Fig. 8. The gravity gradient signatures for the Horst model show a maximum variation of T_{zx} at 40 km and 80 km i.e. the boundaries of the trapezoidal body representing the horst block and maximum value of T_{zz} at the center of the bodies from 40 km to 80 km. To demonstrate the computational algorithm, we have utilized the available gradient data (observed) in comparison to the calculated responses by MATLAB in Fig. 8. From this comparison, it is seen very clearly that the result of this algorithm fit well with the observed data without any other geological or geophysical constraint (Fig. 8a, b and d). In this case, gravity data with tensor gravity gradients may be used directly to depict changes in lithology as well as in providing information on structural systems and deformation style.

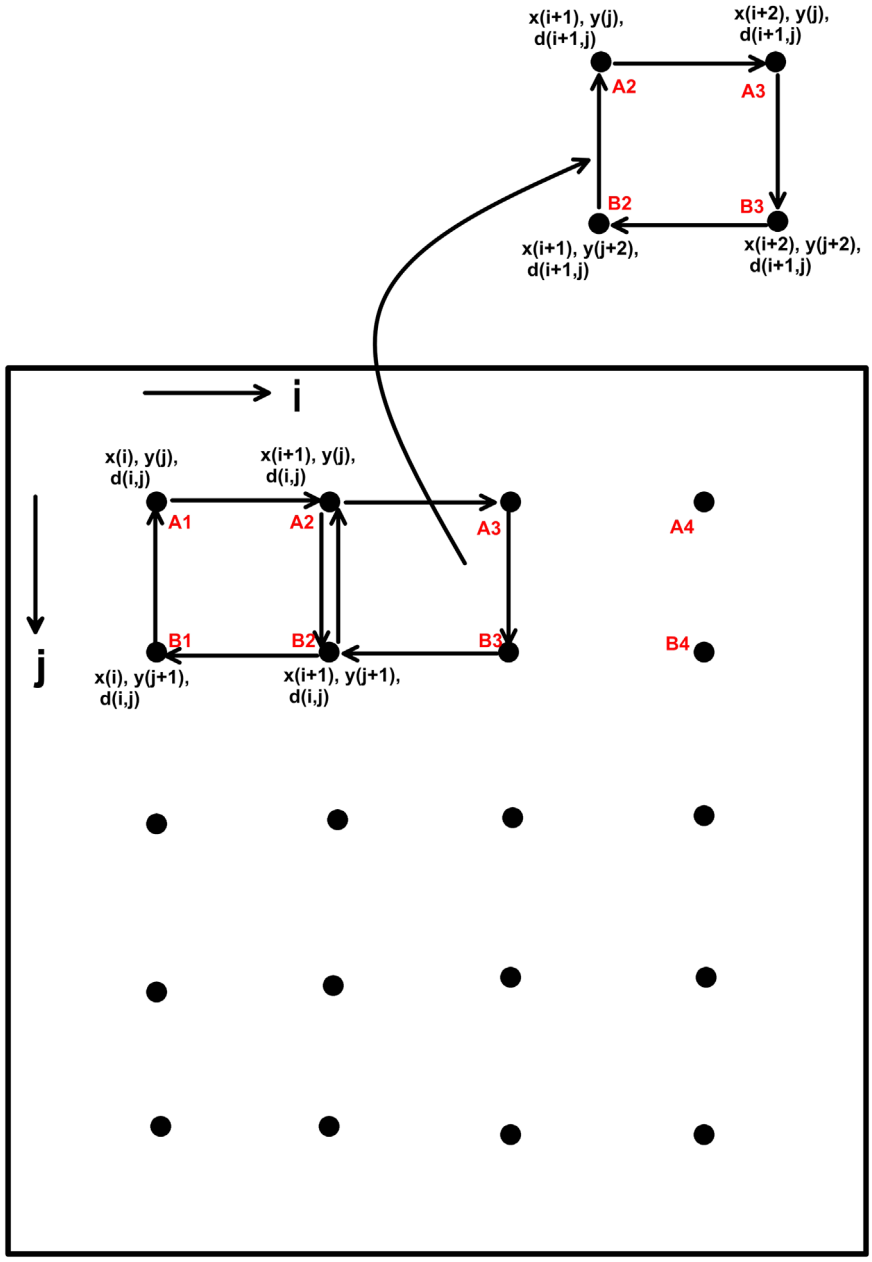

Fig. 6. The algorithm demonstration for the computation of three dimensional undulated layers as shown in Fig. 10 and its gravity gradient behavior.

4.2. Analysis of irregular three dimensional geometries using vertical rectangular prisms or infinite cells: Vredefort Dome, South Africa

The Vredefort impact structure is located in the Witwatersrand basin of South Africa and is known as Vredefort dome (Fig. 9). The structure is one of the largest and oldest known impact structures on the Earth with a diameter of 300 km covered by ~2.02 Ga old rocks and which is known for its economic gold reserves (Salmimen et al., 2010). The geological cross section of the dome reveals two major structures known as core and collar. The core of this dome consists of Archean granitoids and overturned supracrustal strata in the form of a collar pattern (Martinez and Li, 2011). Many geophysical surveys were carried to identify the geological features within the Vredefort dome. One of them includes the gravity gradient data acquired by Fugro Airborne Surveys Corp. using the FALCON Airborne Gravity Gradiometer (Dransfield, 2010).

We have computed the responses of the causative sources approximating the Vredefort dome structure through rectangular geometry to demonstrate the application of the present computation algorithm. A total number of 6539 vertical rectangular prisms with 110 m of element size have been used to build the model using GEOSOFT (OASIS MONTAZ) and then the result was computed by approximating the model with rectangular geometry in MATLAB with model building time of 1.01903 s and CPU time of 0.0624 s. For this purpose, we described a method of approximating the gravity, full gravity gradients of an irregular shaped surface or body representing it as a polyhedron like vertical rectangular prism using MATLAB computational algorithm (*mfile named as irregular.m*). With the aid of analytical formulae derived for the field caused by a finite rectangular prism, a machine method is developed for rapid computation of gravity and full gravity gradient anomalies due to a body of any shape. The example of Vredeforte is provided to demonstrate the applicability, accuracy and speed of the method. In this method, a body is first represented by its top irregular surfaces at different elevations, each elevation representing the upper part of the prism. The body

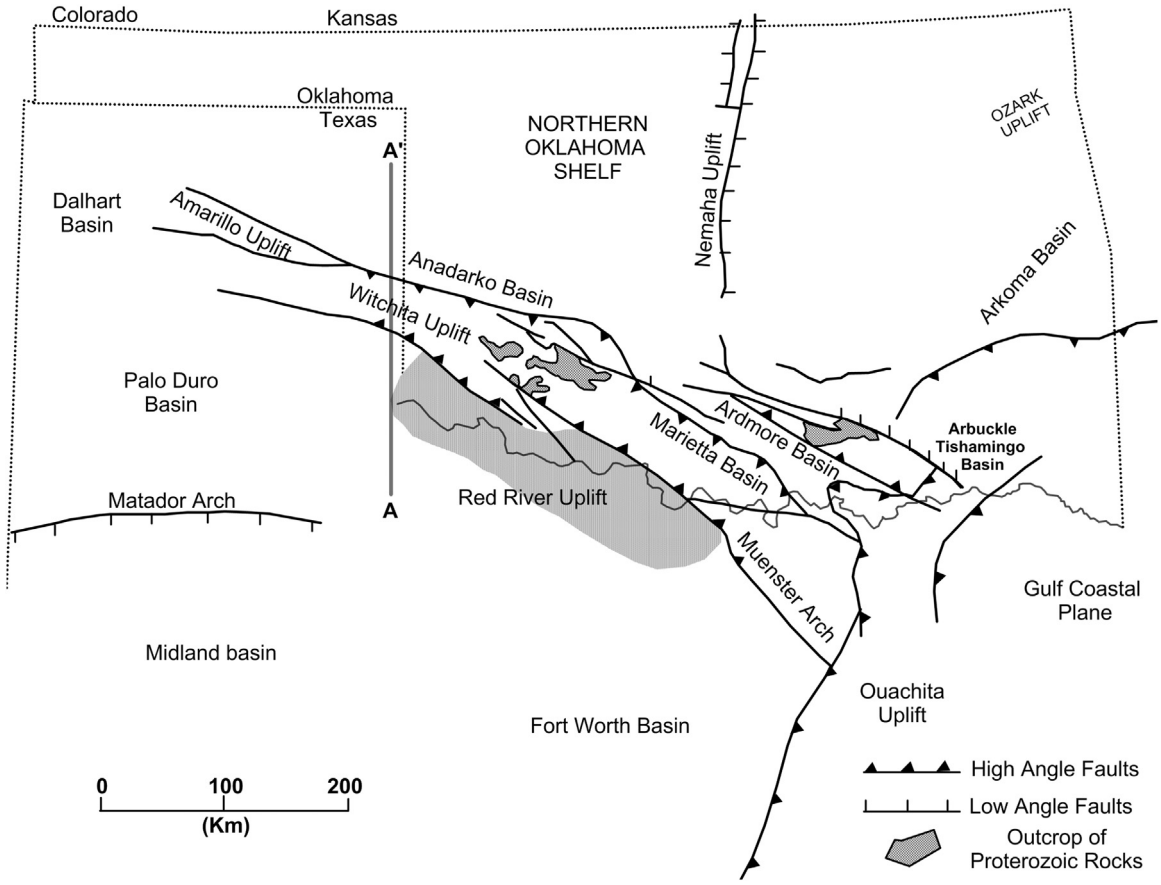

Fig. 7. Major geologic features in part of study area Wichita Uplift, Oklahoma, Texas and Kansas. Line of gravity gradient profile AA′ is also shown in dark gray color from north to south direction.

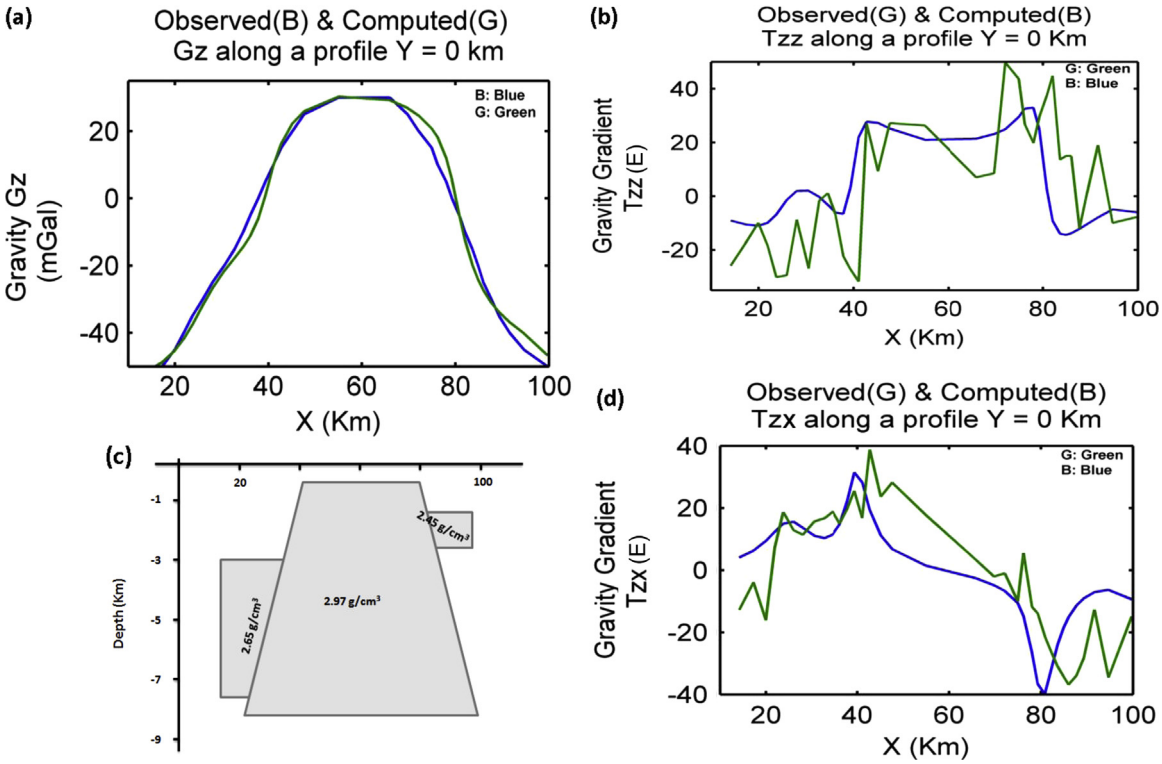

Fig. 8. (a) Calculated and measured vertical gravity component G_z and (b and d) Calculated T_{zz} and T_{xz} components corresponding to the model shown in c: the horst model representing the Wichita uplift with background density of 2.67 g/cm^3.

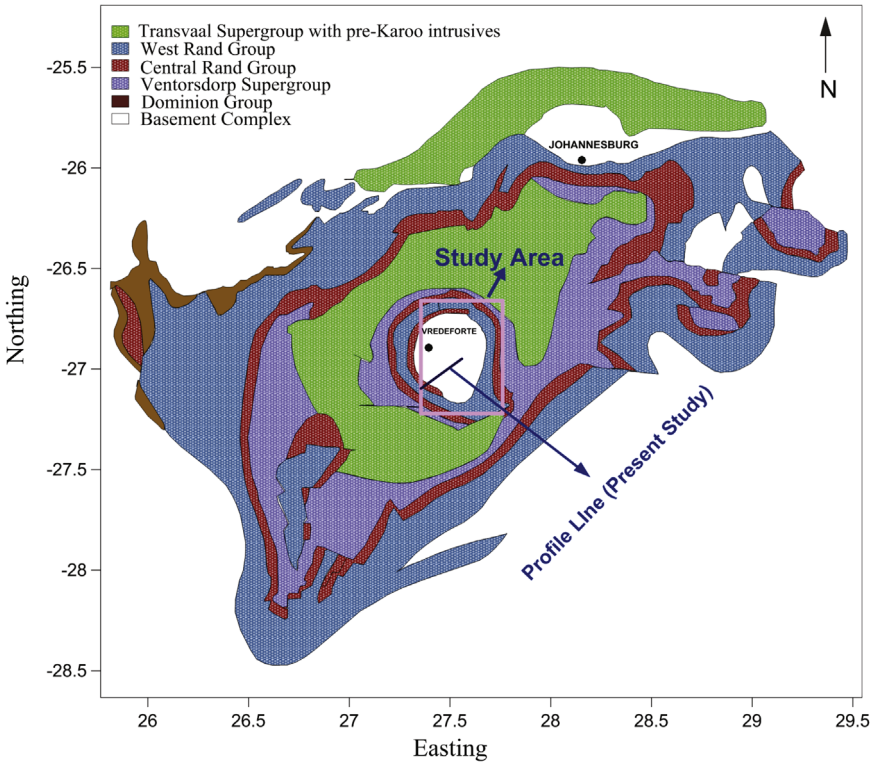

Fig. 9. Geology map of Vredefort impact structure in Witwatersrand basin of South Africa.

is then approximated by a number of rectangular blocks of dimensions similar to top surface samples. Thus in effect, the body is divided into a number of vertical rectangular blocks or infinite cells of small thickness as shown in the Fig. 10. By summing the effects of the total number of blocks, the gravity effect of the whole body is evaluated. Conversely, the method could be utilized for determination of physical parameters from the observed anomalies by inversion process.

Fig. 11a–d illustrate observed and calculated results of G_z and T_{zz} map of Vredefort Dome, South Africa (Dransfield, 2010) using MATLAB computational algorithm. Fig. 12a and b shows the comparison of the observed and computed gravity field and vertical gravity gradient along a profile in NE–SW direction (shown in Figs. 9 and 11) with rms misfit of 3.0845 mGal and 2.0725 mGal/km respectively using 2D model structure of Vredefort Dome along same profile line modeled with a 110 m thickness of rectangular laminae using basement density of 2.97 g/cm^3 and background density to 2.67 g/cm^3 in Fig. 12c. Fig. 12d shows three dimensional view of Vredefort dome generated by GEOSOFT, which was later used to compute the G_z and T_{zz} using rectangular

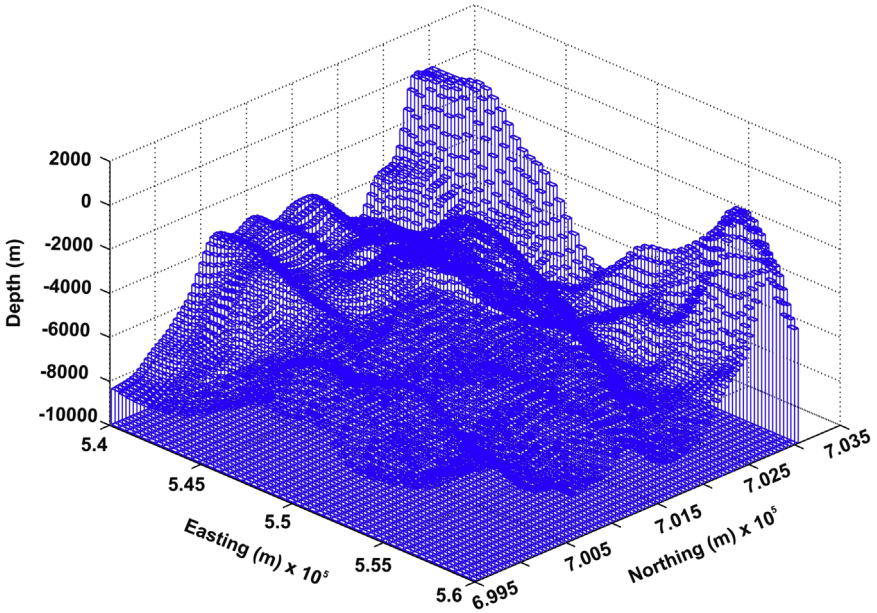

Fig. 10. Approximation of an irregular shaped surface of Vredefort Dome by a number of thin vertical rectangular prisms or infinite cells.

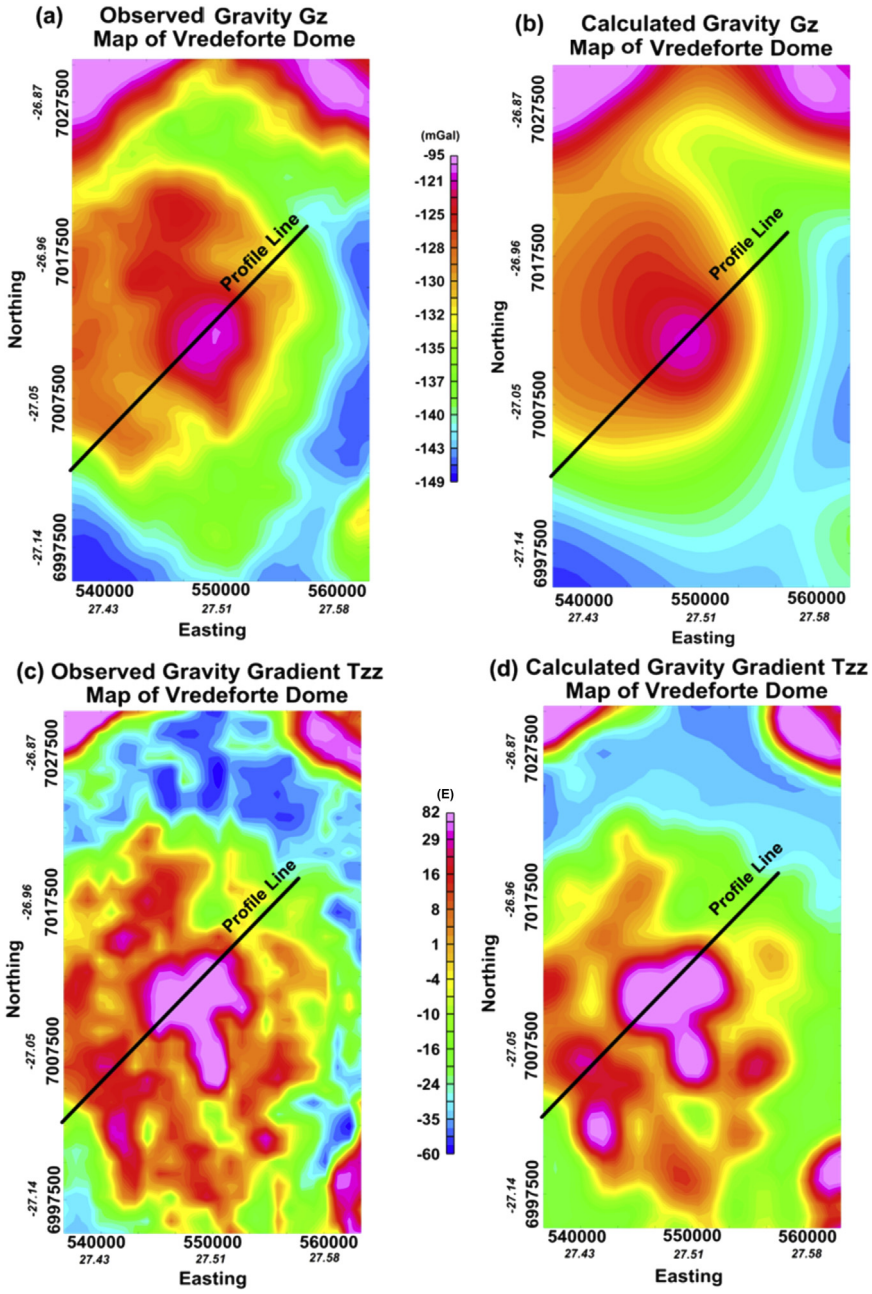

Fig. 11. (a, b) Observed G_z and T_{zz} map of Vredefort Dome, (c, d) computed and observed responses of G_z and T_{zz} for Vredefort Dome as shown in Fig. 12(d).

lamina. Joint modeling of gravity and gravity gradient allowed us to provide a refined geometry of the dome using the presented computational technique. The computational result shows that this technique has the ability to recognize the edge and boundaries of Vredefort Dome with smaller element size and higher resolution.

5. Conclusion

A pattern of complex gravity gradient anomalies is often produced even for simple geometries making difficult the interpretation of observed data. It is easy to understand the complex pattern of gravity gradients through the synthetic models and thus the forward modeling results can be used to guide the interpretation of real gravity and gravity gradient data. Similarly, various combinations of tensor components can be used to produce coordinate independent "invariants" that are simple, easy to interpret, more localized, and more related to the size and shape of the source.

Computational results of rectangular lamina using MATLAB algorithm for forward modeling of gravity and its gradients for simple geometries are found to be same as the IGMAS results with rms error of 0.0198 mGal, 0.0067 eötvos, 0.0151 eötvos and 0.0095 eötvos for gravity field G_z, gravity gradient T_{zx}, T_{zy} and T_{zz} respectively.

Both the geological models presented in the paper indicate that joint modeling of the gravity gradient tensor components greatly improves the determination of the lateral boundaries of the model. The present study is an important step towards understanding the complex nature of gravity gradients, particularly in the view of advent of airborne full tensor gradiometry, which allows mapping shallow and small geological targets, important for exploration. The MATLAB codes can be found as electronic supplementary material.

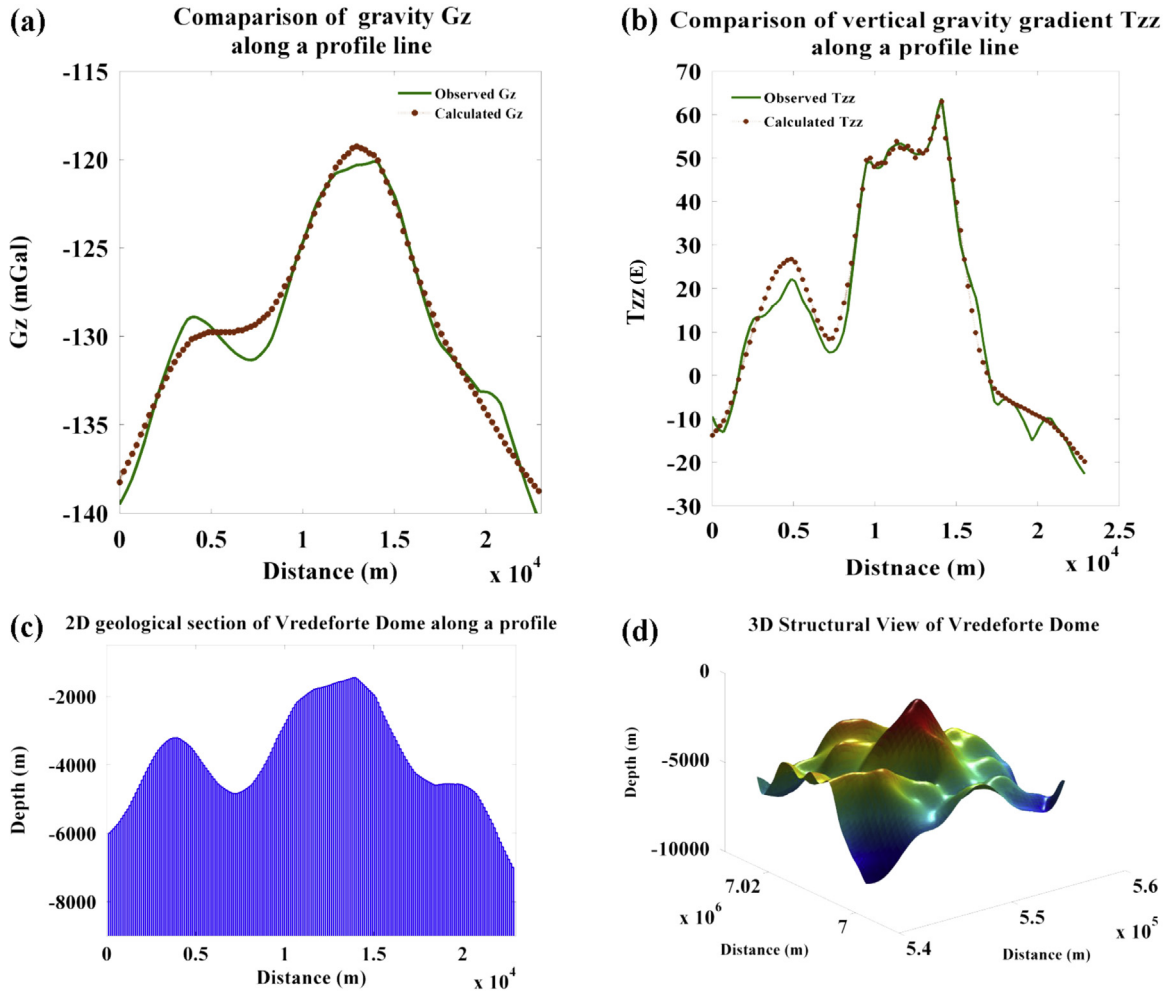

Fig. 12. (a, b) Computed and observed responses of G_z and T_{zz} along a profile in northeast direction as shown in Fig. 11, (c, d) 2D model structure of Vredefort Dome along a profile line modeled with a 110 m thickness of rectangular laminae using basement density of 2.97 g/cm^3 and 2.67 g/cm^3 of background density and 3D structural view of Vredefort Dome.

Acknowledgments

We thank Director, CSIR-NGRI for his permission to publish this paper and one of the authors CPD acknowledges CSIR for providing the Senior Research Fellowship. We greatly appreciate insightful and constructive comments by M. Dransfield that helped to improve the manuscript. We also thank M. Beiki and M.R.K. Prabhakar Rao for their suggestions.

Appendix A

1. Gravity and horizontal gravity gradients of 2D geometries like semi-infinite horizontal slab and vertical sheet/dike (Dransfield, 1994)

A) Semi-infinite horizontal slab

The semi-infinite horizontal slab (bottom left of Fig. 2) is useful for approximating vertical faults. The gravity anomaly and horizontal gradients for such a slab can be calculated by

$$G_z = 2G\rho\left(\frac{\pi t}{2} + x\ln\left(\frac{r_b}{r_t}\right) + (d+t-y)\phi_b - (d-y)\phi_t\right)$$

$$T_{xz} = -2G\rho\ ln\left(\frac{r_b}{r_t}\right)$$

$$T_{zz} = -2G\rho(f_b - f_t)$$

$$r_t = \sqrt{(x^2 + (d-y)^2)}$$

$$r_b = \sqrt{(x^2 + (d+t-y)^2)}$$

$$f_t = \arctan\left(\frac{x}{(d-y)}\right)$$

$$f_b = \arctan\left(\frac{x}{(d+t-y)}\right)$$

B) Vertical sheet/dike

The vertical sheet is useful for modeling dikes. For a vertical sheet (bottom right of Fig. 2) of thickness t and density ρ, the gravity anomaly and its gradients can be calculated by-

$$G_z = 2G\rho t\ ln\left(\frac{r_b}{r_t}\right)$$

$$T_{xz} = 2G\rho t\left(\frac{x}{r_b^2} - \frac{x}{r_t^2}\right)$$

$$T_{zz} = -2G\rho t\left(\frac{(d+l-y)}{r_b^2} - \frac{(d-y)}{r_t^2}\right)$$

$$r_t = \sqrt{\left(x^2+(d-y)^2\right)}$$

$$r_b = \sqrt{\left(x^2+(d+l-y)^2\right)}$$

2. Gravity and gravity gradients of spherical body and vertical cyliNDER (Zhang et al., 2000)

A) Spherical body

The attraction of sphere/point mass buried below earth's surface can be viewed in much the same as the attraction of the entire earth from some distance in space; the formula of gravity and gravity gradients at surface point (upper left of Figs. 3.1 and 3.2) is described below:

where:

$$Gz = \frac{4\pi G\Delta\rho \boldsymbol{R}^3}{3}\frac{z}{r^3}$$

$$Tzz = -\frac{4\pi G\Delta\rho \boldsymbol{R}^3}{3}\frac{2z^2-x^2-y^2}{r^5}$$

$$Tzy = -\frac{4\pi G\Delta\rho \boldsymbol{R}^3}{3}\frac{3yz}{r^5}$$

$$Tzx = -\frac{4\pi G\Delta\rho \boldsymbol{R}^3}{3}\frac{3xz}{r^5}$$

$$Tyy = \frac{4\pi G\Delta\rho \boldsymbol{R}^3}{3}\frac{x^2+z^2-2y^2}{r^5}$$

$$Txx = \frac{4\pi G\Delta\rho \boldsymbol{R}^3}{3}\frac{y^2+z^2-2x^2}{r^5}$$

$$Txy = -\frac{4\pi G\Delta\rho \boldsymbol{R}^3}{3}\frac{3xy}{r^5}$$

R=radius of sphere (m)
$r=\sqrt{x^2+y^2+z^2}$
x, y=horizontal distance from the center (m)
z=depth of sphere (m)

B) Vertical cylinder

The formula of gravity and gravity gradients of a finite vertical cylindrical body at surface point (upper left of Fig. 4) is described below:

$$Gz = \frac{4\pi G\Delta\rho \boldsymbol{R}^3}{3}\frac{z}{r^2}$$

$$Tzz = -\frac{4\pi G\Delta\rho \boldsymbol{R}^3}{3}\frac{z^2-x^2-y^2}{r^4}$$

$$Tzy = -\frac{4\pi G\Delta\rho \boldsymbol{R}^3}{3}\frac{3yz}{r^4}$$

$$Tzx = -\frac{4\pi G\Delta\rho \boldsymbol{R}^3}{3}\frac{3xz}{r^4}$$

$$Tyy = \frac{4\pi G\Delta\rho \boldsymbol{R}^3}{3}\frac{x^2+z^2-y^2}{r^4}$$

$$Txx = \frac{4\pi G\Delta\rho \boldsymbol{R}^3}{3}\frac{y^2+z^2-x^2}{r^4}$$

$$Txy = -\frac{4\pi G\Delta\rho \boldsymbol{R}^3}{3}\frac{3xy}{r^4}$$

where,
R=radius of vertical cylinder (m)
$r=\sqrt{x^2+y^2+z^2}$
x, y=horizontal distance from the center (m)
z=depth of vertical cylinder (m)

3. Gravity and gravity gradients of rectangular lamina

To compute the effects of rectangular laminas that extends from $x=x1$ to $x=x2$, $y=y1$ to $y=y2$, and $z=z1$ to $z=z2$, triple integration is performed with appropriate limits (Upper left of Fig. 5). This has been carried out by numerous authors including Jung (1961), Nagy (1966), Plouff (1976), Barton (1929) and Forsberg (1984). Gravity field can be written as:

$$G_z = G\rho s\sum\sum\sum\left[z_k\tan^{-1}\left\{(x_i{*}y_j)/(z_k{*}r_{ijk})\right\} - x_i\log(r_{ijk}+y_j) - y_j\log(r_{ijk}+x_i)\right]$$

$$G_x = G\rho s\sum\sum\sum\left[x_i\tan^{-1}\left\{(y_j{*}z_k)/(x_i{*}r_{ijk})\right\} - y_j\log(r_{ijk}+z_k) - z_k\log(r_{ijk}+y_j)\right]$$

and

$$G_y = G\rho s\sum\sum\sum\left[z_k\log(r_{ijk}+x_i) + x_i\log(r_{ijk}+z_k) - y_j\tan^{-1}\left\{(z_k{*}x_i)/(y_j{*}r_{ijk})\right\}\right]$$

where
1. G is Gravitational Constant, ρ is Density,
2. i, j, and k are indices labeling the corners of the rectangular lamina along x, y, and z axis respectively
3. $s=1$, if $i+j+k$ is even and $s=-1$, if $i+j+k$ is odd
4. r_{ijk}=sqrt($x_i^2+y_j^2+z_k^2$),

After differentiating the G_x, G_y, and G_z in x, y, and z direction respectively (Talwani, 1965) gravity gradient components can be obtained as shown below in compact forms:

$$T_{xx} = G\rho s\sum\sum\sum\left[(-1){*}\tan^{-1}\left\{(x_i{*}y_j)/(x_i^2+z_k{*}r_{ijk}+z_k^2)\right\}\right]$$

$$T_{xy} = G\rho s\sum\sum\sum\left[(-1){*}\log(r_{ijk}+z_k)\right]$$

$$T_{xz} = T_{zx} = G\rho s\sum\sum\sum\left[0.5{*}\log(r_{ijk}-y_j)/(r_{ijk}+y_j)\right]$$

$$T_{yy} = G\rho s\sum\sum\sum\tan^{-1}\left\{(-1){*}(x_i{*}y_j)/(r_{ijk}^2+z_k{*}r_{ijk}+x_i^2)\right\}$$

$$T_{yz} = T_{zy} = G\rho s\sum\sum\sum\left[0.5{*}\log(r_{ijk}-x_i)/(r_{ijk}+x_i)\right]$$

$$T_{zz} = G\rho s(V_1+V_4)$$

where

$$V_1 = s\sum\sum\sum\tan^{-1}\{(x_{i*}y_j)/(x_i^2+z_{k*}r_{ijk}+z_k^2)\}$$

$$V_4 = s\sum\sum\sum\tan^{-1}\{(x_{i*}y_j)/(r_{ijk}^2+z_{k*}r_{ijk}+x_i^2)\}$$

Appendix B. Supplementary material

Supplementary data associated with this article can be found in the online version at http://dx.doi.org/10.1016/j.cageo.2015.12.007.

References

Barnet, C.T., 1976. Theoretical modeling of the magnetic and gravitational field of an arbitrarily shaped three dimensional body. Geophysics 41 (6), 1353–1364.

Barton, D.C., 1929. Calculations in the interpretation of observations with the Eötvös torsion balance. AIME 81, 481–504.

Bhattacharyya, B.K., 1964. Magnetic anomalies from prism-shaped bodies with arbitrary polarization. Geophysics 29, 517–531.

Bickford, M.E., Lewis, R.D., 1979. U-Pb Geoehronology of Exposed Basement Rocks in Oklahoma. S3. Geological Society of America Bulletin, United States, p. 500-M4.

Coggon, J.H., 1976. Magnetic and gravity anomalies of polyhedra. Geoexploration 14, 93–105.

Dransfield, M., 1994. Airborne Gravity Gradiometry: Unpublished (Ph.D. thesis). University of Western Australia, Australia.

Dransfield, M., 2010. Conforming Falcon gravity and the global gravity anomaly. Geophys. Prospect. 58, 469–483.

Dransfield, M., Christensen, A., 2013. Performance of airborne gravity gradiometers. Lead. Edge 32 (8), 908–922. http://dx.doi.org/10.1190/tle32080908.1.

Dubey, C.P., Gotze, H.J., Schmidt, S., Tiwari, V.M., 2014. A 3D model of the Wathlingen salt dome in the Northwest German Basin from joint modeling of gravity, gravity gradient, and curvature. Interpretation 2 (4), 1–13. http://dx.doi.org/10.1190/INT-2014-0012.1.

Forsberg, R., 1984. A Study of Terrain Reductions, Density Anomalies and Geophysical Inversion Methods in Gravity Field Modeling. Department of Geodetic Science and Surveying, Ohio State University, United States, p. 129, Report No.355.

Götze, H.-J., Lahmeyer, B., 1988. Application of three-dimensional interactive modeling in gravity and magnetics. Geophysics 53 (8), 1096–1108.

Godah, W., Krynski, J., 2011. Validation of GOCE gravity field models over Poland using the EGM2008 and GPS/levelling data. Geoinform. Issues 3 (1(3)), 5–17.

Herceg, M., Tscherning, C.C., Levinsen, J.F., 2014. Sensitivity of Goce gradients on Greenland mass variation and changes in ice topography. J. Geod. Sci. 4, 8–18.

Hjelt, S.E., 1974. The gravity anomaly of dipping prism. Geoexploration 12, 29–39.

Jung, K., 1961. Schwerkraftuerfahren in der Angewandfen Geophysik, Akademische Verlagsgesellschaft, Leipzig.

Keller, G.R., Baldridge, W.S., 1995. The Southern Oklahoma Aulacogen, in Continental Rifts: Evolution, Structure. In: Tectonics, K.H. Olsen (Ed.), 1995. Elsevier, Amsterdam, pp. 427–435.

Martinez, C., Li, Y., 2011, Inversion of regional gravity gradient data over the Vredeforte Impact structure, South Africa. SEG San Antonlo 2011 Annual Meeting.

Mickus, K., Hinojosa, J.H., 2001. The complete gravity gradient tensor derived from vertical gravity data: a Fourier Transform technique. J. Appl. Geophys. 46, 159–174.

Murphy, C.A., Dickinson, J.L., 2009, Exploring exploration play models with FTG gravity data: 11th SAGA Biennial Technical Meeting and Exhibition, pp. 89–91.

Nagy, D., 1966. Gravitational attraction of a right rectangular prism. Geophysics 31, 362–371.

Okabe, M., 1979. Analytical expression for gravity anomalies due to homogeneous polyhedral bodies and translations into magnetic anomalies. Geophysics 44 (4), 730–741.

Pedersen, L.B., Rasmussen, T.M., 1990. The gradient tensor of potential field anomalies: some implications on data collection and data processing of maps. Geophysics 55 1558-1556.

Plouff, D., 1976. Gravity and magnetic fields of polygonal prisms and application to magnetic terrain corrections. Geophysics 41, 727–741.

Pohánka, V., 1988. Optimum expression for computation of the gravity field of a homogeneous polyhedral body. Geophys. Prospect. 36, 733–751.

Saad, A.H., 2006. Understanding gravity gradients – a tutorial. Lead. Edge 25 (8), 942–949.

Salmimen, J.M., Pesonen, L.J., Lahti, K., Kannus, K., 2010, Testing the Origin Of High Remanent Magnetization In Vredeforte Impact Structure: AGU, Fall Meeting 2010.

Schmidt, S., Gotze, H.-J., 1998. Interactive visualization and modification of 3D models using GIS functions. Phys. Chem. Earth 23 (3), 289–295.

Talwani, M., 1965. Computation with the help of a digital computer of magnetic anomalies caused by bodies of arbitrary shape. Geophysics 30, 797–817.

Talwani, M., 2011. Non linear inversion of gravity gradients and the GGI gradiometer. Cent. Eur. J. Geosci. 3 (4), 424–434. http://dx.doi.org/10.2478/s13533-011-0041-3.

Talwani, M., Ewing, M., 1960. Rapid computation of gravitational attraction of three-dimensional bodies of arbitrary shape. Geophysics 25, 203–225.

Tsoulis, D., 2012. Analytical computation of the full gravity tensor of a homogeneous arbitrarily shaped polyhedral source using line integrals. Geophysics 77 (2), F1–F11. http://dx.doi.org/10.1190/GEO2010-0334.1.

Yao, L., Changli, Y., 2007. Forward modeling of gravity, gravity gradients and magnetic anomalies due to complex bodies. J. China Univ. Geosci. 18 (3), 280–286.

Zhang, C., Mushayandebvu, M.F., Reaid, A.B., Fairhead, J.D., Odegard, M.E., 2000. Euler deconvolution of gravity tensor gradient. Geophysics 65 (2), 512–520.

Zuidweg, K., Mumaw, G.R., 2007. Airborne Gravity Gradiometry For Exploration Geophysics – The First Five Years. Bell Geospace Ltd., Unit 5A Crombie Lodge, ASTP Bridge of Don, AB22 8GU Aberdeen, United Kingdom.